IN SITU BUBBLE CHARACTERIZATION DURING RESIN INFUSION FOR PROCESS SIMULATION OF VOIDS

Brock Zobell[1] and Andrew George[1]

[1] School of Technology, Brigham Young University; 265 CTB, BYU, Provo, Utah 84602, USA, andy_george@byu.edu

Keywords: Liquid resin infusion, Voids, Void transport, Image analysis

ABSTRACT

Optimization of liquid composite molding processes would greatly benefit from an understanding of how voids form and move during processing. While theoretical models exist in the literature for such phenomena, little experimental validation exists due to the difficulties of characterizing voids inside the mold, in a fluid state. The best experimental methodologies presented so far involve light transmission and thus only work for fiberglass reinforcements. An experimental methodology is presented in this paper, in which a proper lighting scheme allows for *in situ* photography of bubbles during liquid composite molding of carbon reinforcements. The resulting images were processed using image analysis software to identify key parameters such as grey level threshold, and size and circularity limits, which best allow for automated identification of bubbles in the images. No script achieved complete identification of all of the bubbles, but a methodology was developed and implemented to iterate the analysis parameters, evaluate the resulting bubble identification performance, and identify a range of analysis parameters that would provide the best possible results for automated *in situ* void detection.

1 INTRODUCTION

One of the key factors in a quality composite part is low void content. A void occurs when gas or air bubbles become trapped in the matrix material and remain after final cure of the part. Voids reduce the matrix's ability to transfer loads and create failure points within the laminate. In order for a laminate part to achieve the mechanical properties of its design intent, a minimal void content is required. Prepreg and autoclave cure are the composites manufacturing method associated with the fewest voids. The significantly lower cycle times and cost benefits associated with liquid composite molding (LCM), e.g. resin transfer molding (RTM), make it a tempting alternative to prepreg, but usually entails a higher void content. Void modeling and simulation for infusion processes is a critical step in finding a composites processing solution that can meet current demands for reduced costs, while still meeting mechanical performance requirements [1].

During infusion, two types of voids are created: micro and macro voids. Microvoids can be described as air bubbles trapped within the fiber bundles themselves, while macrovoids are larger bubbles located in the channels between the bundles. These bubbles are created by the mechanical entrapment of air, which is the most common cause of voids in resin infusion processing [2]. Microvoids are created if the inter-bundle flow is faster than capillary-induced flow within the bundles, while the opposite case forms macrovoids. The applied pressure gradient and advancing flow front cause the voids to compress and migrate with the resin flow. Resin flow velocity, fiber tow permeability and fiber orientation of the preform are all variables that affect void formation, compression and migration.

Modeling tools for both bubble formation and bubble movement during infusion are under development [1,3], but little experimental work exists to support and validate such models. Void measurement in a cured laminate is inherently time-consuming. Even more difficult, the validation of models regarding void formation [2,4] requires some way of measuring *in situ* bubble formation at the

moment they are created by mechanical entrapment. Models for bubble mobility [5,6] require *in situ* monitoring of bubbles flowing through the reinforcement. The little documented data that exists focuses on fiberglass [4,7,8] as its transparency facilitates *in situ* bubble measurement. But the high performance industry demanding such simulation tools deals primarily with opaque carbon fibers. While various methods quantifying differences in conductivity [9] and mass flow rate [7,10] have attempted to measure local bubble formation in carbon reinforcements, the accuracy and resolution are inadequate as void content volumetric percentages are low.

Thus, an accurate, repeatable, and rapid method for measuring *in situ* void (bubble) content during infusion is yet desired, especially for carbon fiber reinforcements. This study presents the trial and error work regarding variation in lighting methods, dyes, photographic equipment, tooling, and process conditions all in the effort to allow for imaging of bubbles inside the reinforcement during infusion, for both fiberglass and carbon fibers. The end goal is to enable rapid delivery of micrographs that have sufficient contrast between bubbles and the other components of the composite material and enable automated image analysis of large amounts of photos.

2 METHODOLOGY

A two-piece RTM mold with a cavity measuring 300 x 50 mm (Figure 1) was machined from Polymethyl Methacrylate (PMMA) (both top and bottom pieces). The thickness of the cavity was controlled with thickness gauge spacers and set at the appropriate thickness for ~50% fiber content in the test reinforcement. Inlet and vent ports were machined and fitted on both ends of the cavity. The PMMA is only 25 mm in thickness, but steel c-channel bars were used along the length of the mold to minimize deflection. The camera equipment consisted of a Sony SLTA77V-a77 Digital SLR camera with remote shutter release and a Sigma 50 mm f/2.8 EX DG macro lens. The camera was suspended directly over the tooling with a clear field of view of the fiber preform in an area near the vent, where the most voids were thought to be located.

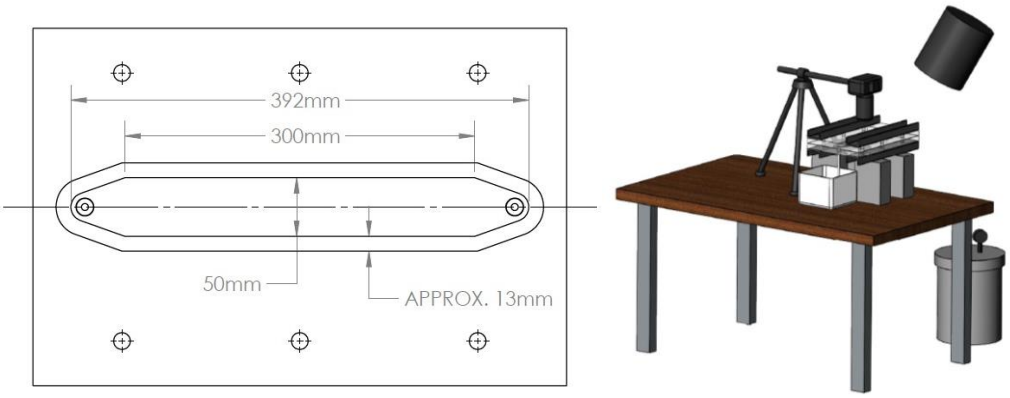

Figure 1: Mold dimensions (left) and experimental setup (right) for *in situ* void characterization during infusion.

Fluid injection was performed on both fiberglass and carbon reinforcements at applied pressures of 150 to 200 kPa. A generic plain weave was chosen as the fiberglass reinforcement for this study. Two carbon reinforcements were studied: a weave (Hexcel 4H satin AGP185-CS, 185 g/m^2) and a +45/-45 biaxial non-crimped fabric (NCF) (VectorPly C-BX 1800, 580 g/m^2). As the flow front advanced, micrograph pictures were taken in rapid succession throughout the infusion process in an effort to capture bubble movement. The bubbles in the micrographs were then analyzed in the free online software Image-J. Various modifications to the test fluid (canola oil, viscosity of 60 mPa·s) and lighting were made in efforts to achieve sufficient contrast between the bubbles and non-bubble material in the resulting micrographs for easy, automated bubble detection. The dye used in some experiments was Dye-Lite TP-3400-0601 (Tracer Products), mixed into the oil at approximately 5% of

the total volume. Viscometer measurements confirmed that the dye caused no significant change to the oil viscosity.

3 RESULTS

3.1 Image Acquisition

The following initial tests were performed, but which all obtained little contrast, i.e. inability to distinguish the bubbles in Image-J:

1. Fiberglass: No light (except normal room lighting) and no dye
2. Fiberglass: No light (except normal room lighting) and a colored dye (to improve bubble to oil contrast)
3. Fiberglass: LED lighting under the (transparent) tooling with no dye
4. Fiberglass: No light (except normal room lighting) and UV dye in the oil
5. Fiberglass: UV lighting under the tooling with UV dye in the oil
6. Fiberglass: UV lighting above the tooling with UV dye in the oil

The transparency of the fiberglass seems to introduce too much light to the bubbles in the above cases, making it difficult to achieve any contrast between the bubbles and the oil. As with a previous study using a similar method [11], bubbles are seen in the images, but there is not enough contrast to automate bubble analysis in Image-J.

Interestingly, when the carbon reinforcement was tested in the last experimental setup described above (UV lighting above the tooling with UV dye in the oil), much better results were achieved. The oil with the UV dye glowing against the dark fibers showed a high contrast between bubbles and the test fluid. Figure 2 demonstrates a micrograph for a single-layer twill weave sample, with red circles denoting some areas of bubbles. The difficulty with detecting the bubbles now moves to discerning them from the likewise dark fibers. Such fibers are darkest when pressed against the PMMA mold wall.

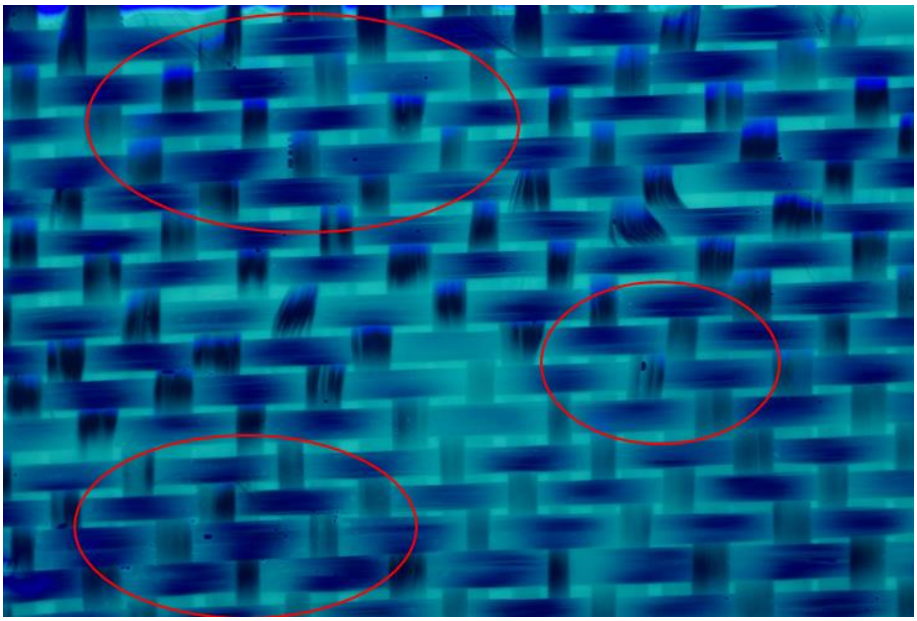

Figure 2: Twill weave during infusion with oil and UV dye, under UV lighting.

The carbon biaxial NCF was then tested. Due to its lower permeability than the twill weave, this afforded more photography time and thus easier characterization. Two plies of the reinforcement were stacked into a laminate for the micrograph in Figure 3, in order to increase the amount of bubbles seen

(projected through the thickness).

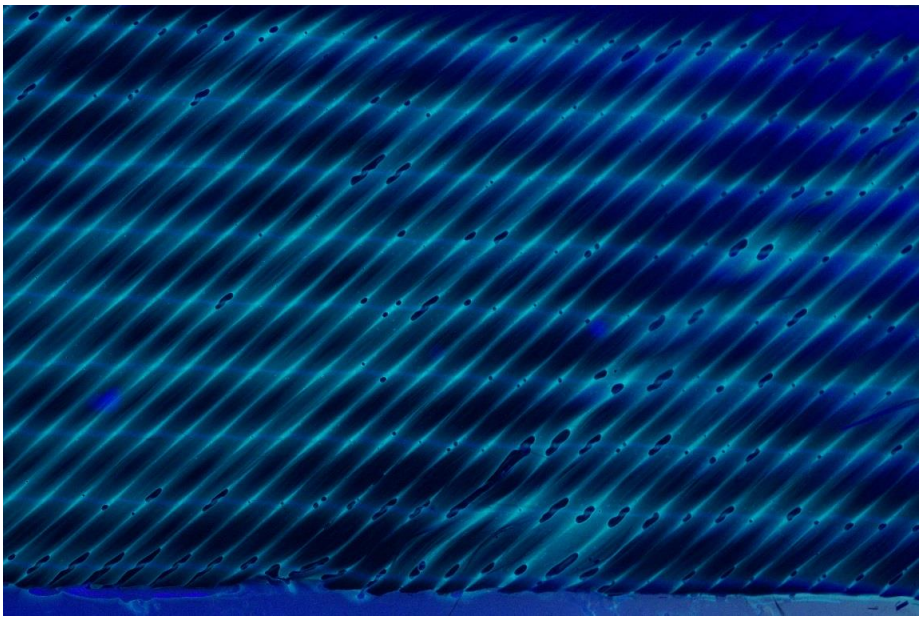

Figure 3: Biax NCF during infusion with oil and UV dye, under UV lighting.

3.2 Image Analysis

Again, the fibers pressing against the mold wall cause areas as dark as the bubbles, thus impeding easy delineation by gray level thresholding in Image-J. As the bubbles are more rounded than the dark fiber areas, the particle analysis tool in Image-J was investigated for its applicability to delineate the bubbles. This tool takes a binary (black and white) image, and looks for circular outlines. It labels each circular object with an ID number, and provides morphology data on each including surface area. For this circularity delineation to succeed, the user must define three important values in the image analysis:

1) the gray level threshold value to make all voids appear as black objects, and as little non-void elements as possible,
2) the range in size (area) of the detected bubbles, which eliminates small specks of background noise in the micrographs, and any larger black areas due to uneven image shading,
3) the minimum circularity of the bubbles, to remove the longer (larger aspect ratio) dark fiber areas.

A shade correction macro (“A Posteriori”) was used on all images to normalize to some degree the background shading in each image. The “enhance contrast” feature was also used on all images to make the bubbles more discernible. These enhancements are shown in Figure 4.

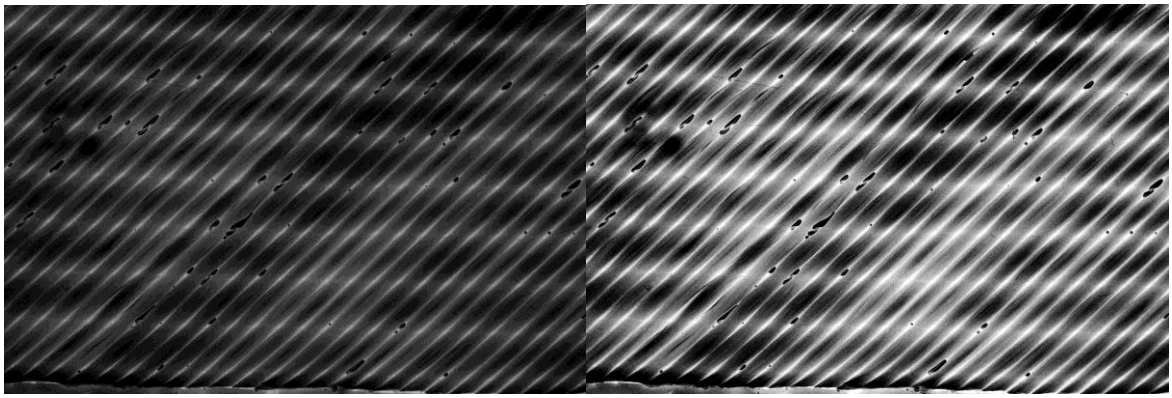

Figure 4: Biax NCF binary image before shading and contrast enhancements (left) and after (right).

The gray level threshold was then adjusted manually, letting progressively lighter shades into the "black" split until all the bubbles appear in the binary image. The particle analysis tool is then run, again manually-adjusting the size and circularity limits to detect as many voids as possible. An example analysis is shown in Figure 5, of a small area in the middle of the micrograph shown in Figure 3, where the detected bubbles are the outlined objects in the right image, and the dark elliptical fiber areas have been removed.

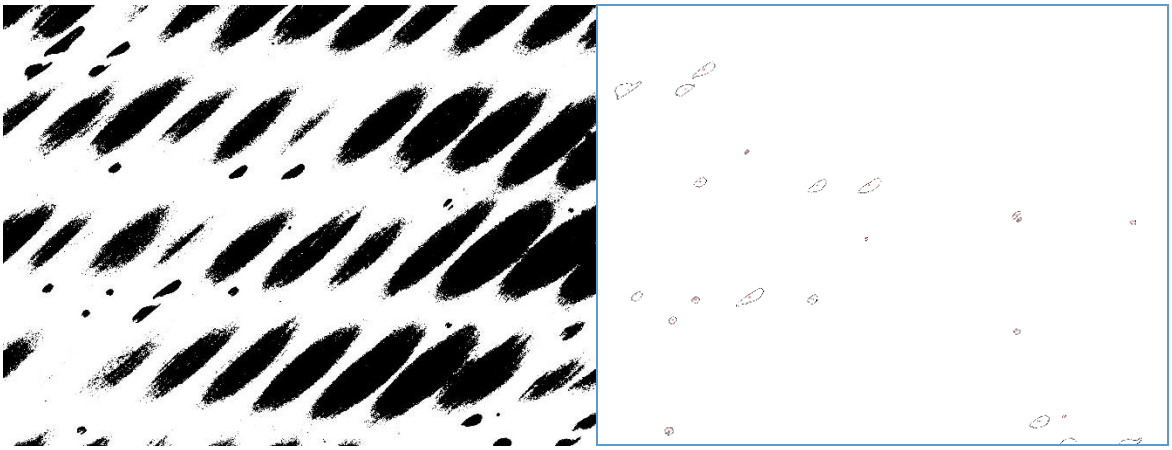

Figure 5: Binary image of dark areas including bubbles and fibers (left) and with size and circularity filters applied in Image-J (right) to leave only bubble shape profiles.

3.3 Automated Image Analysis

The methodology described above allows for an excellent characterization of the *in situ* bubbles during infusion of these carbon reinforcements. But such manual adjustment of all the image analysis parameters to optimize bubble detection is tedious. As the void distribution and morphology is non-uniform (Figure 5), many images must be analyzed to perform a statistical analysis of void distribution and morphology for future process simulation tools. This section outlines efforts in automating the above tasks, so that a series of images could be analyzed at once.

Three sample images from the carbon biax NCF infusions were analyzed as follows. The gray-level threshold, size limits, and minimum circularity values were all iterated with the images, and the resulting map of detected bubbles (e.g. right-side in Figure 5) was evaluated by comparing it with the original image. A 7x7 grid was laid over the original image (Figure 6), and each of the 49 sections was examined by zooming in on it and counting each of the bubbles by eye. The total bubbles in the image was compared against the number of bubbles in the analysis using an effectivity ratio *E*:

$$E = \frac{\left({}^{Rp}/_{Vt}\right)}{\left({}^{Rf}/_{Rt}\right) + 1} \quad (1)$$

R_p = Total number of correctly identified bubbles in image analysis
R_f = Total number of false identified bubbles in image analysis
R_t = Total number of identified bubbles in image analysis
V_t = Total number of bubbles manually counted in the original image

This then not only credits identification of the bubbles, but penalizes the "score," E, for incorrectly identified bubbles.

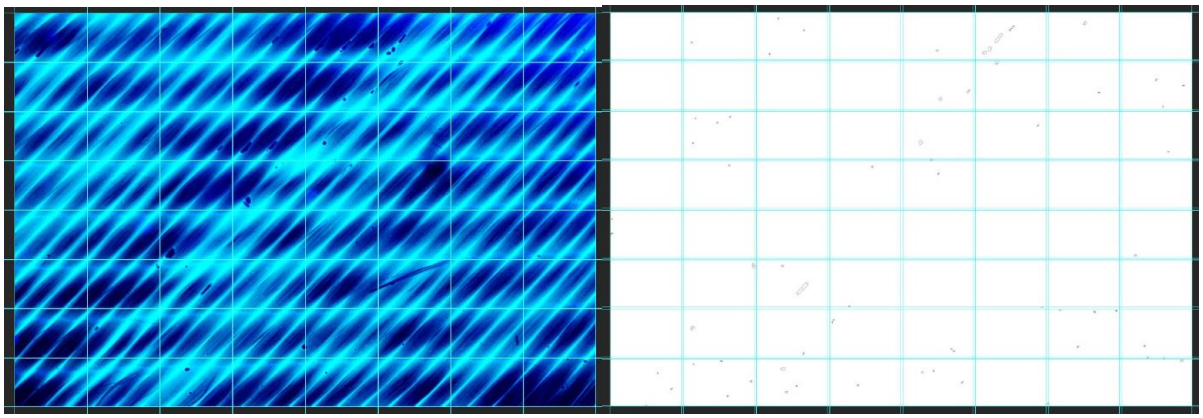

Figure 6: 7x7 grid laid out on original image and bubble map for comparison.

In the image shown in Figure 6, 74 different voids were identified (total areal void content = 0.11 %) and labeled in the original image. Thirteen different permutations of the grey-level threshold, size range, and minimum circularity were attempted. Between the different image analysis settings attempted, 53 of the 74 or 72% of the voids were identified, but no single setting achieved better than 33 of the 74 voids or 45% identified. Most of these settings also included high numbers of false readings ranging from four up to 38. The maximum effectivity ratio achieved was 0.299, at a threshold of 65 (from 0 to 255), size range of 100-10,000 (pixel^2) and circularity range of 0.3-1.0. Most of the larger voids were identified, but over half of the total bubbles were missed.

A second image was then used, with a completely different void distribution, to see if the optimal image analysis settings carried over. In the second image, only seven different voids were identified in the original image (0.02% void content). Eleven different combinations of image analysis settings were attempted with the best one achieving E = 0.857, where only one bubble was missed and no bubbles were incorrectly identified. But this was only achieved with modifications to the optimal gray threshold (103) and size range (150-8,000) from the first image.

The third image again had a large number of voids, many of them being large macrovoids. A total of 77 voids were identified in the original image (void content = 0.5%), and the optimal of 11 permutations of the image analysis settings resulted in E = 0.602. The original and optimal analysis are shown in Figure 7. Again, the optimal threshold setting (140) and size range (100-15,000) were slightly different from previous images.

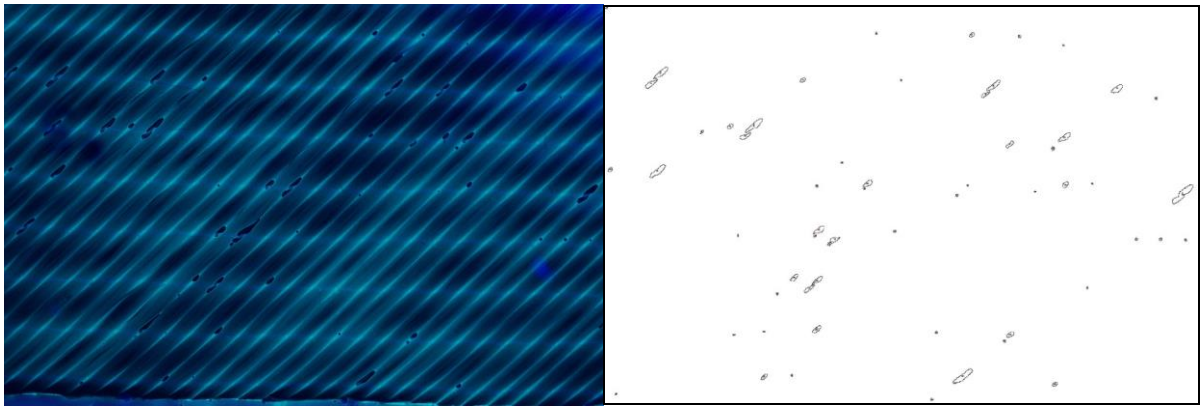

Figure 7: Comparison of third image and optimal settings for bubble detection.

Overall, a circularity range worked well for optimum effectivity (*E*) for the three images, but no universal threshold or size range seemed to work well. A range of settings was identified for the gray threshold and size, however, which could be used in analysis of future images. This suggests that some hand measurement of voids may be necessary, to evaluate and determine approximate settings for automated void measurement. Automated image analysis may never identify 100% of the voids correctly. But the methodology can be optimized to identify as many possible, thus enabling analysis of a large volume of images, e.g. from a video of an infusion experiment, for near continuous monitoring of void formation and movement.

4 CONCLUSIONS

An experimental methodology was developed, in which a proper lighting scheme allowed for *in situ* photography of bubbles during liquid composite molding of carbon reinforcements. The resulting images were processed using image analysis software to identify analysis parameters that best allowed for automated identification of bubbles in the images. No script allowed for complete identification of all of the bubbles, but a methodology was developed and implemented, to iterate the analysis parameters, evaluate the resulting bubble identification performance, and identify a range of analysis parameters that produces the best possible results for automated *in situ* void detection.

REFERENCES

[1] C. Park et al., Modeling and simulation of voids and saturation in liquid composite molding processes, *Composites: Part A*, **42**, 2011, pp. 658-668.

[2] N. Patel and L.J. Lee, Modeling of void formation and removal in liquid composite molding. Part II. Model development and implementation, *Polymer Composites*, **17**, 1996, pp. 104–114.

[3] S. Leclerc and E. Ruiz, Porosity reduction using optimized flow velocity in Resin Transfer Molding, *Composites: Part A*, **39**, 2008, pp. 1859-1868.

[4] F. LeBel et al., Prediction of optimal flow front velocity to minimize void formation in dual scale fibrous reinforcements, *International Journal of Material Forming*, **7**, 2014, pp. 93-116.

[5] V. Frishfelds, T.S. Lundström and A. Jakovics, Bubble motion through non-crimp fabrics during composites manufacturing, *Composites Part A*, **39**, 2008, pp. 243-251.

[6] T. Lundstrom, V. Frishfelds and A. Jakovics, Bubble formation and motion in non-crimp fabrics with perturbed bundle geometry, *Composites: Part A*, **41**, 2010, pp. 83-92.

[7] B. Gourichon, C. Binetruy and P. Krawczak, A new numerical procedure to predict dynamic void content in liquid composite molding, *Composites: Part A*, **37**, 2006, pp. 1961-1969.

[8] R. Matsuzaki, D. Seto, A. Todoroki and Y. Mizutani, Void formation in geometry-anisotropic woven fabrics in resin transfer molding, *Advanced Composite Materials*, **23**, 2014, pp. 99-114.

[9] M. Villiere et al., Experimental study on the identification of saturation of a porous media through thermal analysis, *Proceedings of ICCM19, Montreal, Canada*, 2013, pp. 2218-2227.

[10] J. Verrey, V. Michaud and J. Manson, Dynamic capillary effects in liquid composite moulding with non-crimp fabrics, *Composites: Part A*, 37, 2006, pp. 92-102.

[11] F. Lebel et al., Experimental characterization by fluorescence of capillary flows in dual-scale engineering fabrics, *Textile Research Journal*, **83**, 2013, pp. 1634-1659.